"Exact" classical electron dynamic approach for a free-electron laser amplifier

William H. Louisell,* Juan F. Lam, and Drew A. Copeland
Department of Physics, University of Southern California, Los Angeles, California 90007

William B. Colson
Department of Physics, Stanford University, Stanford, California 94305
(Received 17 April 1978)

We have calculated the gain of a free-electron laser in the small-gain-per-pass limit by using the single-particle model. The electron equations of motion reduce to that of a simple pendulum. As operating levels increase, the theory predicts that by varying the amount of detuning, gain enhancement should occur. In addition, we calculate the electron energy and phase distributions at the output of the amplifier assuming the electrons entering are monoenergetic and have a uniform phase distribution. Above a certain operating level, the theory predicts and explains for the first time the occurrence of discontinuities in both distribution functions. The effect of these discontinuities in storage-ring high-power applications is not yet known.

I. INTRODUCTION

If relativistic electrons are sent along the z axis of a circularly polarized dc magnetic field of period λ_q, the electrons follow nearly helical orbits. Spontaneous radiation is emitted mainly in the forward direction in a narrow cone of mean angle[1-3] $\langle\theta\rangle \sim 1/\gamma$, where $\gamma = (1-\beta^2)^{-1/2}$ and θ is the observation angle measured from the z axis. The radiation is circularly polarized. A spectral analysis of this radiation[2,3] shows a series of emitted frequencies at $l\omega_s$ (l being an integer), where

$$\omega_s = \omega_q/(1-\beta_0\cos\theta), \tag{1.1}$$

where $\omega_q = 2\pi c/\lambda_q$ and $c\beta_0$ is the relativistic incident z component of the electron velocity.

If the pitch angle of the helical orbit is sufficiently small, then the radiation is primarily in a narrow ($l=1$) fundamental frequency line. The spontaneous line-shape factor is given by ($l=1$)

$$[\sin(\pi L\xi/\lambda_q)/\xi]^2, \tag{1.2}$$

where

$$\xi = \omega_s/\omega_q(1-\beta_0\cos\theta) - 1, \tag{1.3}$$

and where $L = N\lambda_q$ is the magnet length. The fractional linewidth is

$$|\delta\omega/\omega_s| = 2\lambda_q/L = 2/N, \tag{1.4}$$

and the total power radiated is given by

$$P = e^4\mu_0 c\gamma_0^2 B_0^2/6\pi m^2 \tag{1.5}$$

(we use mks units throughout). B_0 is the dc magnetic field strength. This power is seen to be proportional to r_0^2, the classical electron radius, given by

$$r_0 = e^2/4\pi\epsilon_0 mc^2 = 2.8\times10^{-15}\ \text{m}. \tag{1.6}$$

The fundamental interaction is Compton scattering.[2]

Madey[4] and his collaborators have demonstrated stimulated amplification of this spontaneous radiation at 10.6 μm ($\gamma_0 mc^2 \sim 24$ MeV, $\lambda_q = 3.2$ cm, $L = 5.2$ m). By enclosing the device in a stable mirror oscillator,[5] they have observed laser action at 3.4 μm ($\gamma_0 mc^2 \sim 43$ MeV). This produced about 15×10^6 W/cm^2 power density in the resonant cavity. For forward-stimulated scattering under these conditions, $\beta_0 = 1 - 1/(2\gamma_0^2) \sim 1$, (1.1) reduces to

$$\lambda_s \cong \lambda_q/2\gamma_0^2, \tag{1.7}$$

where $\omega_s = ck_s$ and $\omega_q = ck_q$. Due to the tunability and possibly high-power outputs, this device is attracting widespread interest.

One of us (W.B.C) has recently written a paper[6] which reviews in some detail the history of the free-electron laser, together with analogous devices including the theories (both quantum mechanical and classical), as well as some of the experimental work. The present work follows the approach used in Ref. 6 and its advantage over a prior approach[7] should be self-evident. The problem is treated completely classically. This work is limited to the situation when the gain per pass is small and the single-particle picture is valid.

II. ELECTRON MOTION AS A PENDULUM

A. Electromagnetic fields

As electrons enter the laser cavity, they are influenced by the radiation and static magnetic fields. We assume the electromagnetic fields consist of a circularly polarized dc magnetic field of period λ_q and a backscattered "signal" field of frequency $\omega_s = ck_s$. In a frame of reference

moving along the z axis at velocity $\beta_0 c \sim c$, under the Weizäcker-Williams approximation[1,8] the dc field looks like a plane electromagnetic wave. In the lab frame, we take the incident and scattered vector potentials to be

$$\vec{A}_\perp = \hat{e}_-[A_i e^{-i(\omega_i t + k_i z)} + A_s(t) e^{-i(\omega_s t - k_s z)}] + \text{c.c.}\,, \quad (2.1)$$

where

$$\hat{e}_\pm = (\hat{x} \pm i\hat{y})/\sqrt{2}\,. \quad (2.2)$$

In terms of the true dc magnetic field, we have the relations

$$A_i = B_0/k_i(1+\beta_0) \equiv B_0/k_q = B_0\lambda_q/2\pi\,, \quad (2.3)$$

$$\omega_i = \beta_0 c k_i = c k_q/(1+\beta_0)\,, \quad (2.4a)$$

or

$$\lambda_i = \lambda_q(1+\beta_0) \sim 2\lambda_q\,. \quad (2.4b)$$

Relations (2.3) and (2.4) follow from the fact that the motion of an electron in the presence of static helical magnetic field should be identical to the one in the presence of an equivalent electromagnetic field.[9]

The amplitude of the scattered wave $A_s(t)$ is slowly varying, so that

$$\left|\frac{\partial^2 A_s}{\partial t^2}\right| \ll \omega_s \left|\frac{\partial A_s}{\partial t}\right|\,. \quad (2.5)$$

B. Electron equations of motion

The Hamiltonian describing the system is given by

$$\frac{\mathcal{H}}{mc^2} = \gamma = \frac{1}{(1-\beta^2)^{1/2}} = \left[1 + \left(\frac{\vec{P}_\perp - e\vec{A}_\perp}{mc}\right)^2 + \left(\frac{P_z}{mc}\right)^2\right]^{1/2}. \quad (2.6)$$

Since x and y are cyclic, we conclude $\vec{P}_\perp$ is a constant of the motion. Further, since transverse momentum spreads are negligible, we let $\vec{P}_\perp = 0$. From the Hamiltonian equations of motion, we obtain immediately (before letting $\vec{P}_\perp = 0$),

$$\vec{\beta}_\perp = -e\vec{A}_\perp(z,t)/mc\gamma\,, \quad \beta_z = P_z/mc\gamma\,, \quad (2.7)$$

$$-\frac{\partial H}{\partial z} = \frac{dp_z}{dt} = -\frac{mc^2}{2\gamma}\frac{\partial}{\partial z}\left(\frac{e\vec{A}_\perp}{mc}\right)^2 = \frac{d}{dt}(mc\gamma\beta_z)\,, \quad (2.8)$$

where by (2.1),

$$\frac{1}{2}\left(\frac{e\vec{A}_\perp}{mc}\right)^2 = \left(\frac{e|A_i|}{mc}\right)^2 + \left(\frac{e}{mc}\right)^2 \times [A_i^* A_s e^{i(kz-\Delta\omega t)} + A_i A_s^* e^{-i(kz-\Delta\omega t)}] + \left(\frac{e|A_s|}{mc}\right)^2, \quad (2.9)$$

where

$$k \equiv k_s + k_i\,, \quad \Delta\omega \equiv \omega_s - \omega_i\,. \quad (2.10)$$

We see from (2.9) that the interference between the incident and scattered wave sets up a traveling wave in the z direction with phase velocity

$$\beta_W \equiv v_W/c = \Delta\omega/ck = (k_s - k_i)/(k_s + k_i) \sim 1\,, \quad (2.11)$$

since $k_s \gg k_i$ by (1.7). Comparison of (2.8) and (2.9) shows that $(e\vec{A}_\perp/mc)^2$ acts like an effective "bunching force" on the electron's z momentum component. Depending on the initial phase of an entering electron, some will be speeded up and some slowed down, causing an electron-density fluctuation. An initially monoenergetic electron beam will become spread in energy. The tendency is for the energy gained by the beam to cancel the energy lost. Net gain of the electromagnetic wave will be achieved if more electrons are slowed down than speeded up in traversing the interaction region.

From (2.1) and (2.7) we easily see that

$$\gamma^2 = \gamma_z^2[1 + (e\vec{A}_\perp/mc)^2] \equiv \gamma_z^2 F\,, \quad (2.12a)$$

where

$$\gamma_z^2 \equiv 1/(1-\beta_z^2)\,. \quad (2.12b)$$

If we let

$$A_i^* A_s = -|A_i||A_s| e^{i(\zeta_0+\varphi)} \quad (2.13)$$

where from now on we let $A_i = |A_i|$ and $A_s = |A_s|$ for simplicity; then (2.9) becomes

$$\frac{1}{2}\left(\frac{e\vec{A}_T}{mc}\right)^2 = \left(\frac{eA_i}{mc}\right)^2 - \left(\frac{e}{mc}\right)^2 \times 2A_i A_s \cos\zeta + \left(\frac{eA_s}{mc}\right)^2, \quad (2.14)$$

where

$$\zeta \equiv kz - \Delta\omega t + \zeta_0 + \varphi\,. \quad (2.15)$$

We see that ζ is the phase of the bunching potential and ζ_0 represents the initial phase of an electron entering at $z = t = 0$ relative to the interference phase.

From (2.6) it follows that

$$\frac{d\gamma}{dt} = \frac{e}{mc}\vec{\beta}\cdot\vec{E} \quad (2.16a)$$

in conjunction with (2.7) and $\vec{E} = -\partial A_\perp/\partial t$ to obtain

$$\frac{d\gamma}{dt} = -\frac{e}{mc}\vec{\beta}_\perp\cdot\frac{\partial A_\perp}{\partial t} = \frac{1}{2\gamma}\frac{\partial}{\partial t}\left(\frac{eA_\perp}{mc}\right)^2. \quad (2.16b)$$

We may combine (2.16b) to eliminate $d\gamma/dt$ from

(2.8). If we also use (2.14) together with the approximation (2.5), we obtain

$$\frac{d\beta_z}{dt} = -\left(\frac{e}{mc\gamma}\right)^2 2A_i A_s kc(1-\beta_z\beta_w)\sin\zeta \ . \qquad (2.17)$$

If we use (2.15), we see that

$$\frac{d\zeta}{dt} = kc\beta_z - \Delta\omega = kc[\beta_z(t) - \beta_w] \ . \qquad (2.18)$$

Thus $d\zeta/dt$ measures the deviation of the electron velocity from the "bunching"-wave phase velocity or the "detuning." Furthermore, we see that

$$\frac{d^2\zeta}{dt^2} = kc\frac{d\beta_z}{dt} \qquad (2.19)$$

is proportional to the z component of the electron acceleration. Combining (2.19) and (2.17) and using the fact that $\beta_w(t) \sim \beta_w \sim 1$, we may rewrite (2.17) as[2,6]

$$\frac{d^2\zeta}{dt^2} \equiv -\Omega^2 \sin\zeta \ , \qquad (2.20)$$

where

$$\Omega^2 \equiv 2(ek_s/m)^2(A_i A_s/\gamma^2\gamma_z^2) \ , \qquad (2.21)$$

which is approximately linearly dependent on the magnitude of the dc magnetic field as well as the scattered field amplitude.

It is convenient to introduce a dimensionless time τ by

$$\tau = ct/L \ , \qquad (2.22)$$

as well as a dimensionless operating-field-strength parameter

$$\epsilon = \Omega L/c \ . \qquad (2.23)$$

Thus (2.20) becomes

$$\frac{d^2\zeta}{d\tau^2} = -\epsilon^2 \sin\zeta \equiv \frac{\partial V_{\text{eff}}}{\partial\zeta} \ , \qquad (2.24)$$

the well-known pendulum equation. In the limit of infinitesimal gain, ϵ is substantially constant (to one part in 10^4 for Stanford operating parameters). However, as energy is transferred to the electromagnetic wave, $A_s^2(t)$ increases and consequently, ϵ grows. In the early Stanford experiments, gain was about 7% which means that ϵ changed by about 7% during the amplification process. Neglecting this change is the most serious approximation in (2.24), and future experiments will probably demonstrate even more gain. The point of the approach presented here is to emphasize the essential physics of the gain process and the electron dynamics in the free-electron laser. As noted in Ref. 6, the pendulum equation describes the slow evolution of the electron's z motion. Electrons do not evolve significantly in the transverse direction.

In dimensionless variables

$$\zeta = k(z - \beta_w L\tau) + \zeta_0 \ , \qquad (2.25)$$

$$\frac{d\zeta}{d\tau} = kL[\beta_z(\tau) - \beta_w] \ . \qquad (2.26)$$

We define

$$\mu \equiv kL[\beta_z(0) - \beta_w] \ , \qquad (2.27)$$

which is proportional to the deviation of the incident-beam velocity from the bunching-wave velocity. We shall use the term resonance or synchronism to correspond to the case $\mu = 0$. In this case there will be no gain, as we shall see.

Much physical insight may be gained from a study of the pendulum equation. A first integral yields

$$\frac{1}{2}\left(\frac{d\zeta}{d\tau}\right)^2 - \epsilon^2\cos\zeta = E \equiv \frac{\mu^2}{2} - \epsilon^2\cos\zeta_0 \ , \qquad (2.28)$$

where μ is given by (2.27) and ζ_0 is the initial electron phase relative to the bunching field. The first term is the analog of the pendulum potential energy. It should be emphasized that E is *not* the electron's energy. $d\zeta/d\tau$ measures the electron-velocity deviation from the bunching-wave phase velocity, while ζ measures the electron phase relative to the bunching field. The pendulum energy E is evaluated in terms of μ and ζ_0 in (2.28). From Fig. 1 we see that for physical motion to occur, $E \geq -\epsilon^2$. For $-\epsilon^2 \leq E_1 \leq \epsilon^2$, bound pendulum orbits occur. In this case, electrons (in the moving frame) oscillate stably in phase from fixed $-\zeta_1$ to $+\zeta_1$ about $\zeta = 2n\pi$, where n is an integer. For $E_2 > \epsilon^2$, the electrons ride over the wave crests, as a pendulum overshoots the top.

Further physical insight may be gained from a "phase-space" plot of $d\zeta/d\tau$ vs ζ. For this let us rewrite (2.28)

$$\left(\frac{d\zeta}{d\tau}\right)^2 = (2k\epsilon)^2\left(1 - \frac{1}{k^2}\sin^2\frac{\zeta}{2}\right) \ , \qquad (2.29)$$

where

$$k \equiv \left[\left(\frac{\mu}{2\epsilon}\right)^2 + \sin^2\frac{\zeta_0}{2}\right]^{1/2} = \frac{E}{2\epsilon^2} + \frac{1}{2} \ . \qquad (2.30)$$

"Closed" or bound orbits occur for $0 \leq k \leq 1$, while "open" orbits occur when $k > 1$. In Fig. 2, we sketch the "phase-space" diagram of the orbits for one period in the ζ direction. The critical orbit corresponds to $k = 1$, viz.,

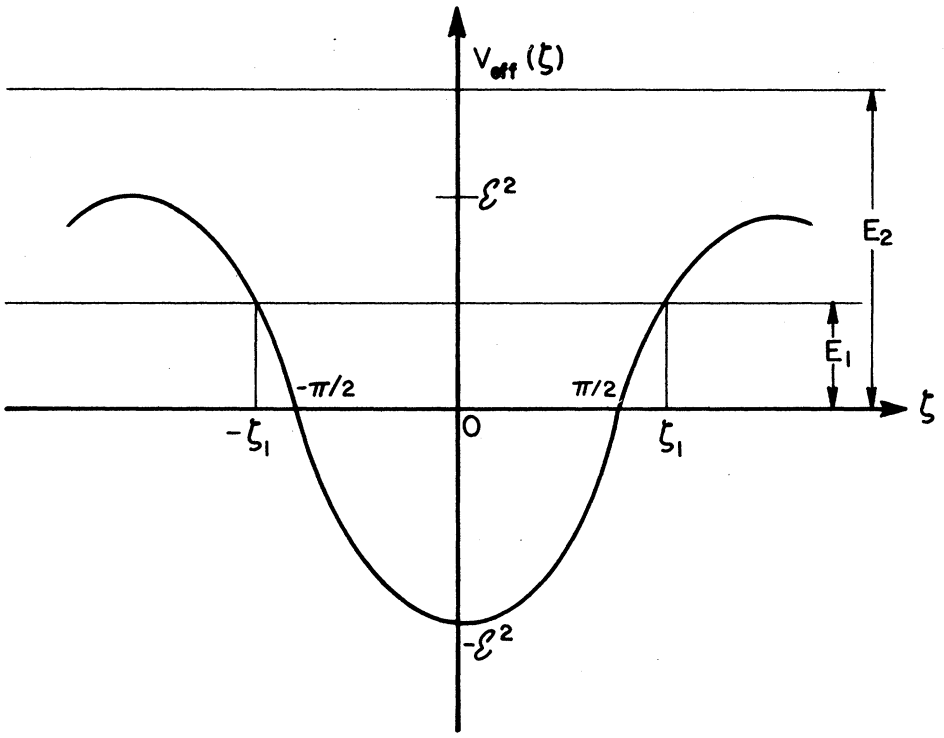

FIG. 1. Effective potential, $V_{eff}=\epsilon^2\cos\zeta$, for electron motion from the simple pendulum model.

$$\frac{d\zeta}{d\tau} = \pm 2\epsilon \cos\frac{\zeta}{2} \ . \tag{2.31}$$

The parameters μ and ζ_0 (for a given field operating level ϵ) determine the orbit in phase space for a given electron. [These are the two initial conditions for the solution of (2.24).]

As seen from Fig. 2 and (2.30), when $\mu > 2\epsilon$ we obtain only open orbits for which $d\zeta/dt > 0$. As $d\zeta/d\tau$ increases, by (2.26), electrons gain energy from the field, and as $d\zeta/d\tau$ decreases they lose energy to the field. A similar argument applies when $\mu < -2\epsilon$ and all orbits are open. This corresponds to the small-signal regime $(\mu/2\epsilon)^2 \gg 1$, or by (2.30) $k^2 \gg 1$. When $(\mu/2\epsilon)^2 < 1$, we see in Fig. 2, as well as (2.30), that some orbits are open and some closed, depending on the initial electron phase ζ_0.

C. Solutions of the equations of motion

Case 1: $k^2 > 1$ open orbits. Except for the case $\mu = 0$, there will always be some open orbits. From (2.29), we see that if $\mu > 0$, the exact solution is

$$\sin\tfrac{1}{2}\zeta = \mathrm{sn}(w, 1/k) \ , \tag{2.32}$$

where $\mathrm{sn}w$ is the Jacobi elliptic function and

$$w \equiv k\epsilon\tau + F(\tfrac{1}{2}\zeta_0, 1/k) \ , \tag{2.33}$$

where

$$F(\phi, k) = \int_0^{\phi} \frac{d\sigma}{(1 - k^{-2}\sin^2\sigma)^{1/2}} \tag{2.34}$$

is the elliptic integral of the first kind. From (2.32) it follows that

$$\frac{d\zeta}{d\tau} = 2k\epsilon \,\mathrm{dn}(w, 1/k) \ , \tag{2.35}$$

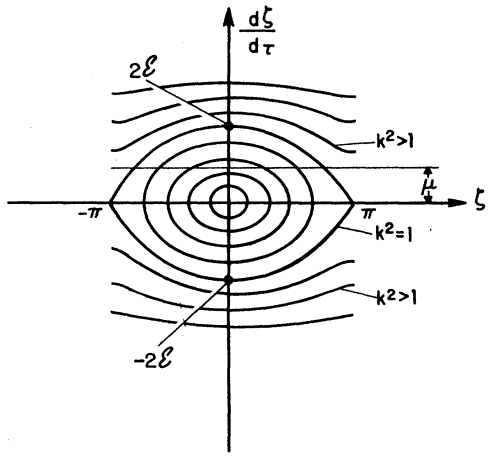

FIG. 2. Phase-space plot of electron orbits. Each contour corresponds to a constant value of the "energy" E. The closed "orbits" have values of $k^2 < 1$ (large-signal regime) while open orbits have values of $k^2 > 1$ (small-signal regime).

where

$$\mathrm{dn}^2 w \equiv 1 - k^{-2}\,\mathrm{sn}^2 w \quad . \tag{2.36}$$

For $\mu<0$ and $k^2>1$ the signs of (2.32) and (2.35) are reversed.

Case 2: $k^2<1$ closed orbits. In this case the solution of (2.29) is

$$\sin\tfrac{1}{2}\zeta = k\,\mathrm{sn}(u,k)\ , \tag{2.37}$$

where

$$u = \epsilon\tau + F(\phi_0, k) \tag{2.38}$$

and

$$\phi_0 = \sin^{-1}(\sin\tfrac{1}{2}\zeta_0/k)\ . \tag{2.39}$$

Also

$$\frac{d\zeta}{d\tau} = 2k\epsilon\,\mathrm{cn}(u,k)\ , \tag{2.40}$$

where

$$\mathrm{cn}^2 u = 1 - \mathrm{sn}^2 u\ . \tag{2.41}$$

Note that

$$\frac{d\zeta}{d\tau}(0) = 2k\epsilon\,\mathrm{cn}(u_0,k) = \mu\ , \tag{2.42}$$

where

$$u_0 = F(\phi_0, k)\ . \tag{2.43}$$

D. Gain and saturation

In contrast to techniques used in Ref. 7 to obtain the gain and saturation which involved the solution of the Maxwell equations coupled to the collisionless Boltzman equation, here we calculate the electron-energy loss and equate it to the field gain, a much simpler procedure as we shall see. The realization that the electron-beam dynamics is not seriously affected by Coulomb repulsion, or collective effects, which will be shown in a forthcoming paper, allows the use of a simpler single-particle description of the free-electron laser.

The average energy lost per electron in traversing the magnet from $\tau=0$ to 1 (at the end of the magnet) is

$$\Delta E = mc^2[\langle\gamma(0)\rangle - \langle\gamma(1)\rangle]\ , \tag{2.44}$$

where we average over all initial phases, assumed uniformly distributed initially; i.e.,

$$\langle\{\ \}\rangle \equiv \frac{1}{2\pi}\int_{-\pi}^{\pi} d\zeta_0\{\ \}\ . \tag{2.45}$$

This phase average is appropriate for any short-wavelength laser, since it is impossible to prepare an electron beam "prebunched" at optical wavelengths. An important result of this work is to show how self-bunching can occur.[2,6]

By energy conservation, the energy lost by the electron beam is assumed to amplify the radiation density. Gain ($\mathcal{G}$) in a section of the electron beam of volume V is taken to be the fractional increase in the radiation energy in that volume, and is given by

$$\mathcal{G} = mc^2\{\langle\gamma(0)\rangle - \langle\gamma(1)\rangle\}\frac{n_e V}{\epsilon_0|E_s|^2 V}\ , \tag{2.46}$$

where n_e is the electron density and $\epsilon_0|E_s|^2$ is the scattered energy density. V is the beam volume. Since

$$|E_s|^2 \equiv 2\omega_s^2|A_s|^2\ , \tag{2.47}$$

$$\mathcal{G} = \frac{m\{\langle\gamma(0)\rangle - \langle\gamma(1)\rangle\}n_e}{2\epsilon_0 k_s^2|A_s|^2}\ . \tag{2.48}$$

By (2.12) and (2.26),

$$\frac{\gamma(\tau)}{(F)^{1/2}} = \left[1 - \left(\frac{1}{kL}\frac{d\zeta}{d\tau} + \beta_w\right)^2\right]^{-1/2}$$

$$\cong \gamma_w\Big/\left[1 - \frac{2\beta_w\gamma_w^2}{kL}\frac{d\zeta}{d\tau}\left(1 + \frac{1}{2kL\beta_w}\frac{d\zeta}{d\tau}\right)\right]^{1/2} \tag{2.49}$$

But $\beta_w\sim\beta_0\sim 1$, $\gamma_w\sim\gamma_0$, $k = k_s + k_i \sim k_s$, and by (1.7) and (2.4b)

$$k_i \cong k_s/4\gamma_0^2\ , \tag{2.50}$$

so that

$$\frac{\gamma(\tau)}{\gamma_0(F)^{1/2}} \cong \left[1 - \frac{1}{2k_i L}\frac{d\zeta}{d\tau}\left(1 + \frac{1}{2k_s L}\frac{d\zeta}{d\tau}\right)\right]^{-1/2}\ . \tag{2.51}$$

For the Stanford experiments $(1/2k_sL)(d\zeta/d\tau)\ll 1$. Thus

$$\mathcal{G} \cong \frac{mn_e\gamma_0(F)^{1/2}}{4\pi\epsilon_0 k_s^2 A_s^2} \times\int_{-\pi}^{\pi}\left[\left(1 - \frac{\mu}{2k_i L}\right)^{-1/2} - \left(1 - \frac{1}{2k_i L}\frac{d\zeta}{d\tau}\right)^{-1/2}\right]d\zeta_0\ . \tag{2.52}$$

Case 1: $(2\epsilon/\mu)\ll 1$ (small signal). In this case the integration may be done analytically.[2] The result is

$$\mathcal{G} = -\frac{mn_e\gamma_0(F)^{1/2}}{2\epsilon_0 k_s^2|A_s|^2}\frac{\epsilon^4}{4k_i L}\frac{d}{d\mu}\left(\frac{\sin\frac{1}{2}\mu}{\mu}\right)^2\ . \tag{2.53}$$

This result is plotted for $\epsilon=0.1$ in Fig. 3, normalized to unity at $\mu=2.6$, the detuning for maximum

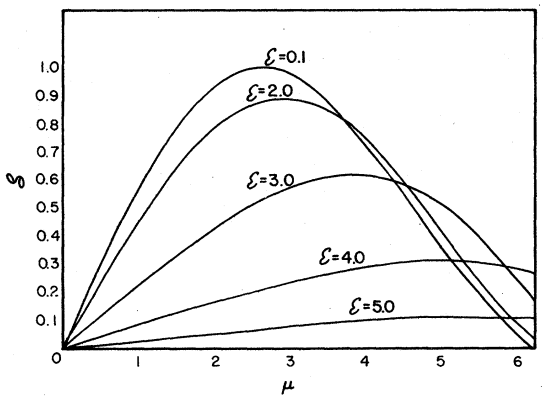

FIG. 3. Gain-saturation S plotted vs electron-velocity detuning μ, for pump parameter $\epsilon = 0.1, 2, 3, 4, 5$. Above threshold, the maximum gain is shifted to higher values of μ.

gain. The plot was done by carrying out the integration of (2.52) using the exact solutions which agree with (2.53), as well as other published results.[6-8] The normalization factor is

$$g_{\max} = \frac{0.675 m n_e \gamma_s (F)^{1/2}}{2\epsilon_0 k_s^2 |A_s|^2} \frac{\epsilon^4}{4k_i L}, \tag{2.54}$$

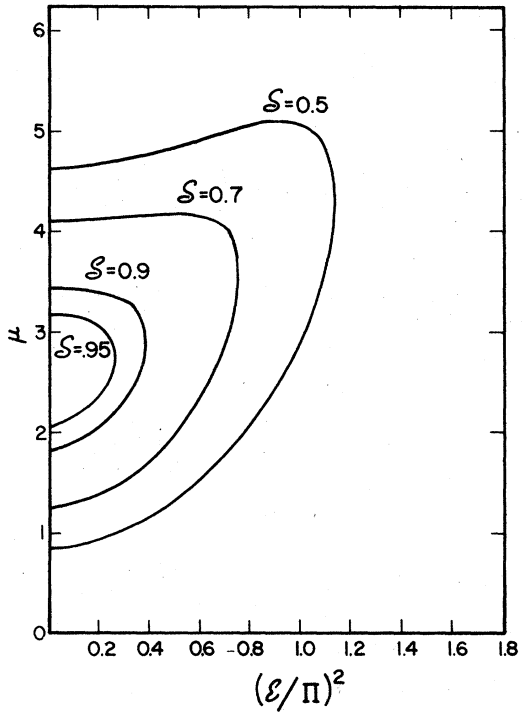

FIG. 4. Contours of constant gain (S) vs detuning and pump parameter $(\epsilon/\pi)^2 = \sqrt{R}$ of Refs. 7 and 9. The shift in the maximum gain vs detuning of Fig. 3 gives the asymmetry shown above and not found in these references.

the maximum small-signal gain.

Case 2: $2\epsilon/\mu \geq 1$ (saturation regime). If we write (2.52) with this normalization, we obtain

$$\mathcal{G} = g_{\max} S,$$

where the saturation function S is given by

$$S = \frac{4}{0.675} \frac{k_i L}{\epsilon^4} \frac{1}{2\pi} \times \int_{-\pi}^{\pi} \left[\left(1 - \frac{\mu}{2k_i L}\right)^{-1/2} - \left(1 - \frac{1}{2k_i L} \frac{d\zeta(1)}{d\tau}\right)^{-1/2} \right] d\zeta_0. \tag{2.55}$$

These are shown in Fig. 3 for $\epsilon = 2, 3, 4$, and 5. We note that as we pump harder, the gain decreases for a given detuning μ, but some gain may be recovered by varying the detuning.

In Fig. 4 we plot contours of constant saturation S versus detuning μ and power level $(\epsilon/\pi)^2$. These are in agreement with Ref. 9. The present calculation detected the error in Ref. 7. The μ here corresponds to the variable μL of Ref. 7 and $(\epsilon/\pi)^2$ to $\sqrt{R}$. In contrast to Ref. 7, the contours are not symmetric about the $\mu = 2.6$ line. The asymmetry in Fig. 4 is due to the shift in maximum gain with μ shown in Fig. 3, which did not show up in the earlier more difficult calculation.

III. EVOLUTION OF THE ELECTRON-ENERGY DISTRIBUTION FUNCTION

The future prospects of a working storage-ring free-electron laser depend upon the behavior of the energy distribution of the electron beam after a single pass through the laser cavity. One defines the electron-beam-energy distribution function at time τ as the probability that the electron energy will be between $mc^2\gamma$ and $mc^2(\gamma + d\gamma)$, i.e.,

$$f_E(\gamma, \tau) d\gamma = \frac{n_e}{2\pi} \int_{-\pi}^{\pi} d\zeta_0 \delta[\gamma - \gamma(\tau, \zeta_0)] d\gamma, \tag{3.1}$$

where

$$\gamma(\tau, \zeta_0) \approx \gamma_0 \sqrt{F} \Big/ \left(1 - \frac{1}{2k_i L} \frac{d\zeta}{d\tau}\right)^{1/2} \equiv \gamma_B \Big/ \left(1 - \frac{1}{2k_i L} \frac{d\zeta}{d\tau}\right)^{1/2}. \tag{3.2}$$

We assume initially all electrons are monoenergetic and distributed uniformly in phase. If we let

$$g \equiv \gamma - \gamma_B \Big/ \left(1 - \frac{1}{2k_i L} \frac{d\zeta}{d\tau}\right)^{1/2}, \tag{3.3}$$

we obtain

$$f_E(\gamma,\tau)=\frac{n_e}{2\pi}\int_{-\pi}^{\pi} dg\ \frac{\delta(g)}{|dg/d\zeta_0|}$$
$$=\frac{n_e}{2\pi}\sum\left(\left|\frac{dg}{d\zeta_0}\right|_{g=0}\right)^{-1}, \tag{3.4}$$

where for fixed γ/γ_w, we sum over all values of $|dg/d\zeta_0|^{-1}$ evaluated at each $\zeta=\zeta_{0n}$ for which

$$\frac{\gamma}{\gamma_B}=\left[1-\frac{1}{2k_i L}\frac{d\zeta}{d\tau}(\tau,\zeta_{0n})\right]^{-1/2} \tag{3.5}$$

where $(-\pi\le\zeta_{0n}\le\pi)$. Or, given γ/γ_w, we find all roots ζ_{0n} for which

$$\frac{d\zeta}{d\tau}(\tau,\zeta_{0n})=2k_i L\left[1-\left(\frac{\gamma_B}{\gamma}\right)^2\right]. \tag{3.6}$$

By (3.3), it follows that

$$\left|\frac{dg}{d\zeta_0}\right|=\left|\frac{\gamma_B}{2[1-(1/2k_i L)d\zeta/d\tau]^{3/2}}\frac{1}{2k_i L}\frac{d}{d\zeta_0}\left(\frac{d\zeta}{d\tau}\right)\right|_{g=0}$$
$$=\frac{\gamma_B}{4k_i L}\left(\frac{\gamma}{\gamma_B}\right)^3\left|\frac{d}{d\zeta_0}\frac{d\zeta}{d\tau}\right|_{g=0} \tag{3.7}$$

or

$$f_E(\delta\gamma,\tau)=\frac{n_e 2k_i L}{\pi\gamma_B}\left(\frac{\gamma_B}{\gamma}\right)^3\sum_n\left[\left|\frac{d}{d\zeta_0}\left(\frac{d\zeta}{d\tau}\right)\right|\right]^{-1}_{g(\zeta_{0n})=0}, \tag{3.8}$$

where

$$\delta\gamma=\left[\frac{\gamma(\tau)}{\gamma_B}-\left(1-\frac{\mu_i}{2k_i L}\right)^{-1/2}\right]\frac{\mu 2k_i L}{\epsilon^2}, \tag{3.9}$$

which is proportional to the energy deviation of the beam from its initial value.

Case 1: $k^2>1$. By (2.35) it follows that

$$\frac{1}{2\epsilon}\frac{d}{d\zeta_0}\left(\frac{d\zeta}{d\tau}\right)=-\frac{\epsilon}{\mu}\,\mathrm{sn}w\,\mathrm{cn}w+\frac{\sin\zeta_0}{4k}\left\{\mathrm{dn}w-\frac{\mathrm{sn}w\,\mathrm{cn}w}{k}\left[\epsilon\tau-\frac{1}{k^2-1}\left(kE\left(\frac{\zeta_0}{2},\frac{1}{k}\right)-\frac{\epsilon\sin\zeta_0}{\mu}\right)+\frac{1}{k}F\left(\frac{\zeta_0}{2},\frac{1}{k}\right)\right]\right\}, \tag{3.10}$$

where

$$E(\phi,k)=\int_0^{\phi}(1-k^2\sin^2\sigma)^{1/2}\,d\sigma\ . \tag{3.11}$$

Case 2: $k^2<1$.

$$\frac{1}{2\epsilon}\frac{d}{d\zeta_0}\left(\frac{d\zeta}{d\tau}\right)=-\frac{\mu}{4k\epsilon}\,\mathrm{sn}u\,\mathrm{dn}u+\frac{\sin\zeta_0}{4k}$$
$$\times[\mathrm{cn}u-\mathrm{sn}u\,\mathrm{dn}u\,kI(\zeta_0)], \tag{3.12a}$$

where

$$kI(\zeta_0)\equiv\frac{1}{1-k^2}\left[E(\phi_0,k)-\frac{\mu}{2\epsilon}\tan\frac{\zeta_0}{2}\right]-F(\phi_0,k) \tag{3.12b}$$

and

$$\phi_0=\sin^{-1}(\sin\tfrac{1}{2}\zeta_0/k)\ . \tag{3.13}$$

If we use in the small signal regime[6] $(2\epsilon/\mu)^2\ll 1$ to the lowest order in $(\epsilon/\mu)^2$, we obtain

$$f_E(\delta\gamma,\tau)=\frac{n_e}{\pi\Delta\gamma}\left(\frac{\gamma_B}{\gamma}\right)^2(\sin^2\tfrac{1}{2}\mu\tau-(\delta\gamma)^2)^{-1/2}, \tag{3.14}$$

where

$$\Delta\gamma\equiv\epsilon^2\gamma_B/\mu 2k_i L\ . \tag{3.15}$$

Hence up to order $(\epsilon/\mu)^2$, an initially monoenergetic electron beam interacting with the radiation fields A_i and A_s will have an equal number of electrons losing energy to the field A_s, as well as an equal number gaining energy from it. This balance condition is reflected in the symmetrical behavior of $f_E(\delta\gamma,\tau)$ as a function of $\delta\gamma$ [Eq. (3.14)]. One can say that, up to order $(\epsilon/\mu)^2$, no net gain has been achieved.

An extension of the small-signal calculation to order $(\epsilon/\mu)^4$ shows that the behavior of $f_E(\delta\gamma,\tau)$ as a function of $\delta\gamma$ is no longer symmetrical.[6] The asymmetry in $f_E(\delta\gamma,\tau)$ implies a net gain has resulted from the interaction process. A plot of the exact $f_E(\delta\gamma,\tau=1)$ from (3.8) for $\epsilon=0.1$ and $\mu=2.6$ is shown in Fig. 5. The asymmetry, which is not visible in Fig. 5, can be understood by looking at Fig. 6. The only contributions to the exact $f_E(\delta\gamma,\tau)$ are the two intercepts of the line γ/γ_B with the function $d\zeta/d\tau$. These two roots, which enter in the denominator of Eq. (3.8) are slightly asymmetric about $\zeta_0=0$ and give rise to a net nonzero gain.

Figure 7 shows a plot of f_E for $\epsilon=0.5$, $\mu=2.6$ (maximum small-signal gain) begins to show slightly more asymmetry toward negative $\delta\gamma$, indicating more electrons lose energy than gain energy. The approximate analytic expression (3.14) is the dotted curve from Ref. 6, and the solid curve is the exact solution. A slight deviation is beginning to show up for this value of the pump parameter ϵ.

As soon as μ becomes less than 2ϵ, both open- and closed-type orbits occur. As may be seen by a comparison of (3.10) $(k^2>1)$ and (3.12) $(k^2<1)$, one sees there must be a discontinuity in the dis-

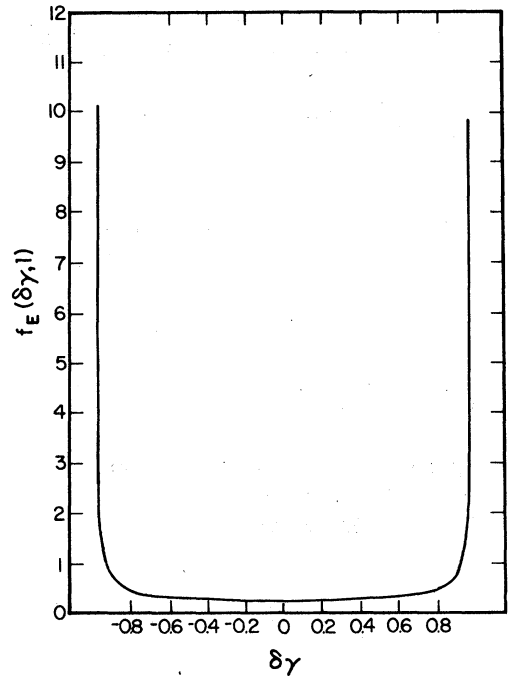

FIG. 5. Output electron-energy distribution function is plotted vs the electron-energy change for $\epsilon = 0.1$ and $\mu = 2.6$ (small-signal maximum gain). An initial δ function centered at $\delta\gamma = 0$ is split into two δ functions. The slight asymmetry (not visible here) is responsible for the gain.

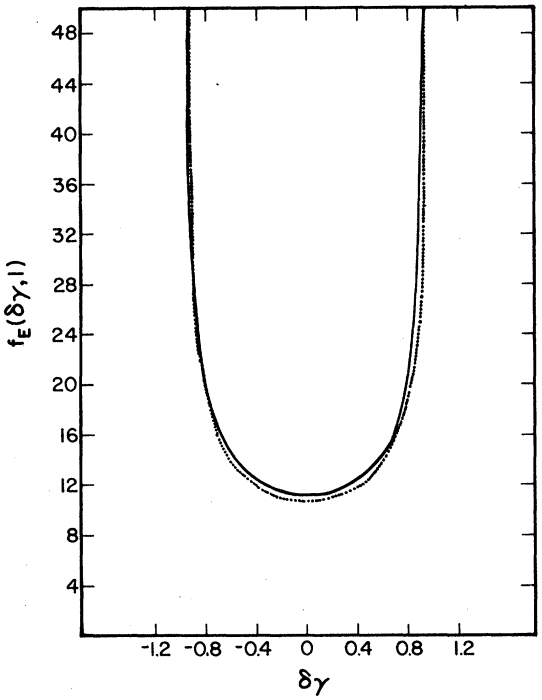

FIG. 7. Energy distribution vs $\delta\gamma$ (electron-energy gain or loss) for $\epsilon = 0.5$, $\mu = 2.6$ (small signal). The agreement between the approximate analytical small-signal calculation (solid curve) and the exact calculation (dotted curve) is still very good. The asymmetry is not yet detectible on the above scale.

tribution function when k goes through the value 1. Figure 8 shows this clearly. With $\mu = 2.7$ (for maximum gain), we plot f_E for $2\epsilon = 2.6$ ($k^2 > 1$) plotted as the solid line which shows the discontinuity (located at $\delta\gamma \simeq -0.75$), while for $2\epsilon = 2.8$, ($k^2 < 1$) plotted as dots show no discontinuity. The asymmetry in the δ functions is now clearly visible, and saturation is beginning to set in.

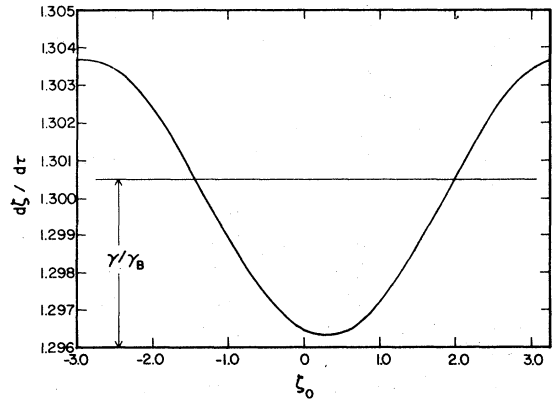

FIG. 6. Plot of $d\zeta/d\tau$ vs initial phase ζ_0 for $\epsilon = 0.1$, $\mu = 2.6$. For a fixed $d\zeta/d\tau$, two values of ζ_0 contribute to the electron-energy distribution function.

In addition to the discontinuities which arise when k changes from open to closed orbits, there are others. In Fig. 9 we plot the energy distribution for the case $\epsilon = 5$, $\mu = 3$ which shows additional discontinuities. These arise at $\delta\gamma \sim -0.6$ and $\delta\gamma \sim +0.05$ because the number roots which contribute to the energy distribution function change from 2 to 4 at $\delta\gamma \sim -0.6$ and from 4 to 2 at $\delta\gamma \sim 0.05$. The discontinuity at $\delta\gamma \sim 0.15$ is due to k changing from less than to greater than 1. This may be clearly seen from Fig. 10, where we plot $d\zeta/d\tau$ aside from a multiplicative constant at the output $\tau = 1$ vs ζ_0. The ζ_0's for which $d\zeta/d\tau$ is a fixed value determine the points which contribute to the energy distribution. For some ranges of $d\zeta/d\tau$, there are four roots, while for some ranges there are two. At these points discontinuities occur. In Fig. 6, where k was always greater than 1, there were always exactly two roots for fixed γ_B/γ (or fixed $d\zeta/d\tau$) so no such discontinuities arise.

The steep rise in $d\zeta/d\tau$ at $\zeta_0 \sim 2.5$ in Fig. 10 may easily be explained by reference to Fig. 11. There we follow two electron orbits with $\mu = 3$ and with an initial $\zeta_0 \sim -2.5$ plotted as a solid ($k \ll 1$) and an open square ($k > 1$). At the output ($\tau = 1$)

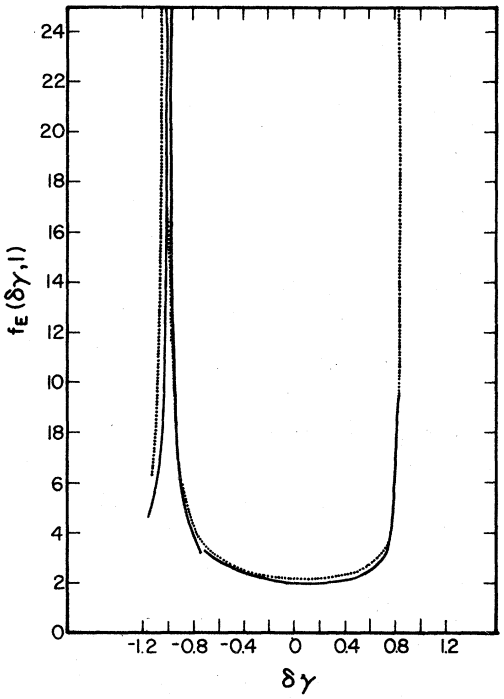

FIG. 8. Electron-energy distribution function vs $\delta\gamma$ for a case in which $k^2>1$ for all ζ_0 (solid curve) and for a case in which k^2 can be less than 1 (dotted curve). The latter case shows a discontinuity when k^2 changes from less than 1 to greater than 1, as predicted by the theory.

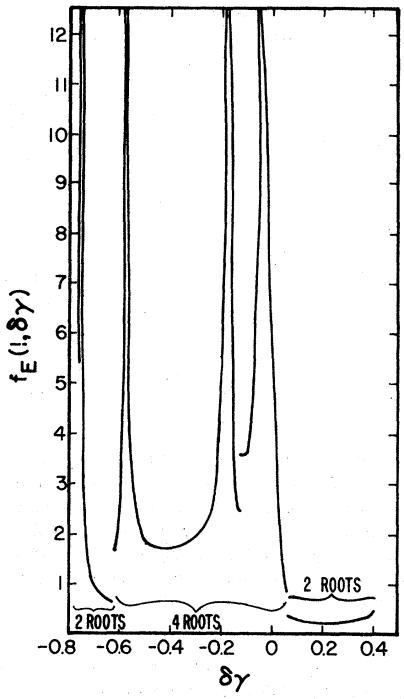

FIG. 9. Energy distribution function vs $\delta\gamma$ for $\epsilon=5$ and $\mu=3$. For $\delta\gamma<-0.6$ and >0.05 there are two roots that contribute to the distribution function while for $-0.6\leq\delta\gamma\leq+0.05$ there are four. The discontinuity at $\delta\gamma\cong-0.13$ is due to k changing from less than 1 to greater than 1.

they both end up near each other ($\zeta\sim3$) in phase space. In this region, Fig. 10 shows $d\zeta/d\tau$ is a slowly varying function of ζ_0. We next follow two electrons with $\mu=3$ and, initially near $\zeta\cong+2.5$. One ($k^2<1$) is plotted as a solid triangle and ends up at $\tau=1$ at $d\zeta/d\tau\cong-8.5$, while the other ($k^2>1$) is plotted as a solid circle and ends up at $\tau=1$ with $d\zeta/d\tau\sim+10$. They are thus far apart in phase space, although their initial conditions were approximately the same. In the limit as $k\to1$, they must end up at the same point in phase space and hence the abrupt rise.

IV. EVOLUTION OF THE ELECTRON PHASE DISTRIBUTION FUNCTION

The pendulum equation allows one in principle to determine the position of an electron at the exit of the interaction region given the initial conditions. We have assumed that the electrons are initially monenergetic and that their phases are uniformly distributed. Following the definition of the energy distribution, the electron phase distribution function is

$$f_p(\theta,\tau)=\frac{n_e}{2\pi}\int_{-\pi}^{\pi}\delta[\theta-\theta(\tau,\zeta_0)]\,d\zeta_0\,, \tag{4.1}$$

where

$$\theta(\tau,\zeta_0)\equiv\zeta(\tau,\zeta_0)-\mu\tau\equiv\theta_0\,. \tag{4.2}$$

The phase distribution is equivalent to a z-po-

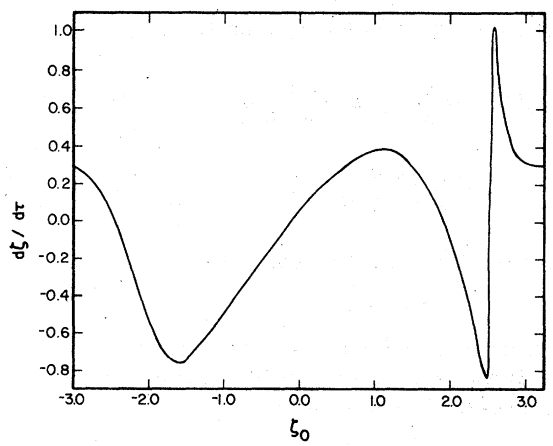

FIG. 10. Plot of $d\zeta/d\tau$ vs ζ_0 for $\epsilon=5$ and $\mu=3$ at the output. For some fixed values of $d\zeta/d\tau$, there are two values of ζ_0, while for other values of $d\zeta/d\tau$ there are four values of ζ_0, which contribute to and explain other energy distribution function discontinuities when k^2 can be less than 1.

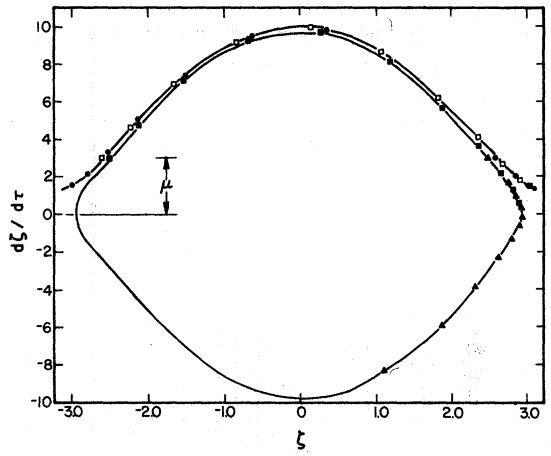

FIG. 11. Orbits for two electrons with initial $\zeta \sim -2.5$ (solid square and open square), which end up at $\tau = 1$ near each other in phase space, as opposed to two electrons with initial $\zeta \sim +2.5$ (solid circle and solid triangle), which at $\tau = 1$ end up at $d\zeta/d\tau \sim +9$ and -8, respectively. This accounts for the steep portion of the curve in Fig. 10 near $\zeta_0 \cong 2.5$.

sition distribution within a wavelength of light in the electron beam. Each section of the electron beam at intervals of one radiation wavelength, evolve identically in phase space. Note that at $\tau = 0$,

$$\theta(0, \zeta_0) = \zeta_0 , \tag{4.3}$$

so that

$$f_p(\theta, 0) = n_e/2\pi , \tag{4.4}$$

which is uniform. Also note that

$$\int_{-\pi}^{\pi} f_p(\theta, \tau)\, d\theta = n_e . \tag{4.5}$$

Let $g = \theta - \theta(\tau, \zeta_0) \equiv \theta - \theta_0$; therefore,

$$f_p(\theta, \tau) = \frac{n_e}{2\pi} \int dg\, \frac{\delta(g)}{|dg/d\zeta_0|} , \tag{4.6}$$

$$= \frac{n_e}{2\pi} \sum \left(\left| \frac{d\zeta}{d\zeta_0} \right| \right)^{-1}_{g=0} . \tag{4.7}$$

That is, for fixed θ we solve for the ζ_{0n} roots of

$$\zeta(\tau, \zeta_0) = \theta - \mu\tau . \tag{4.8}$$

Because of the multivalued nature of (4.8) [see (2.32) and (2.37)], we consider another equivalent phase distribution function

$$f_p(\theta, \tau) = \frac{n_e}{2\pi} \int_{-\pi}^{\pi} \delta\left[\sin\left(\frac{\theta - \theta_0}{2} \right) \right] \left| \cos\left(\frac{\theta - \theta_0}{2} \right) \right| \frac{d\zeta_0}{2} , \tag{4.9}$$

where

$$\theta_0 \equiv \theta(\tau, \zeta_0) \equiv \zeta(\tau, \zeta_0) - \mu\tau . \tag{4.10}$$

Let

$$h = \sin\tfrac{1}{2}(\theta - \theta_0) , \qquad \left| \frac{dh}{d\theta} \right| = \left| \frac{dh}{d\theta_0} \right| ; \tag{4.11}$$

therefore,

$$f_p(\theta, \tau) = \frac{n_e}{2\pi} \int \delta(h) \left| \frac{dh}{d\theta_0} \right| d\zeta_0 . \tag{4.12}$$

Note that at $t = 0$, $\theta_0 \equiv \zeta_0$, so that

$$f_p(\theta, 0) = \frac{n_e}{2\pi} \int \delta(h)\, dh = \frac{n_e}{2\pi} , \tag{4.13}$$

which is uniform. To check normalization at τ, we see that

$$\int_{\theta_0 - \pi}^{\theta_0 + \pi} f_p(\sigma, \tau) d\sigma$$

$$= \frac{n_e}{2\pi} \int_{-\pi}^{\pi} d\zeta_0 \int \delta(h) \left| \frac{dh}{d\theta} \right| d\theta = n_e . \tag{4.14}$$

Thus

$$f_p(\theta, \tau) = \frac{n_e}{2\pi} \int \frac{\delta(h)}{|d\theta_0/d\zeta_0|}\, dh , \tag{4.15}$$

or

$$f_p(\theta, \tau) = \frac{n_e}{2\pi} \sum \frac{1}{|d\zeta/d\zeta_0|_{h=0}} , \tag{4.16}$$

which is seen to be equivalent to (4.7). Thus we want the values of ζ_{0n} for fixed $-\pi < \theta < \pi$ for which

$$h = \sin\tfrac{1}{2}(\theta - \theta_0) = 0 . \tag{4.17a}$$

or by (4.10),

$$\tan\tfrac{1}{2}\theta_0 = \tan\tfrac{1}{2}\theta = \frac{\sin\tfrac{1}{2}\zeta - \cos\tfrac{1}{2}\zeta \tan\tfrac{1}{2}\mu\tau}{\cos\tfrac{1}{2}\zeta + \sin\tfrac{1}{2}\zeta \tan\tfrac{1}{2}\mu\tau} . \tag{4.17b}$$

The roots of (4.8) and (4.17) (i.e., $\theta = \theta_0$) are equal modulo 2π. And since we only need $(d\zeta/d\zeta_0)$ for $g = 0$ or $h = 0$, the modulo 2π cancels. Thus the two distributions are indistinguishable.

Case 1: $k^2 > 1$. From (2.32), we want roots (ζ_{0n}) for fixed θ for which

$$\tan\tfrac{1}{2}\theta = \frac{\mathrm{sn}(w, 1/k) - \mathrm{cn}(w, 1/k) \tan\tfrac{1}{2}\mu\tau}{\mathrm{cn}(w, 1/k) + \mathrm{sn}(w, 1/k) \tan\tfrac{1}{2}\mu\tau} . \tag{4.18}$$

These roots are used to evaluate

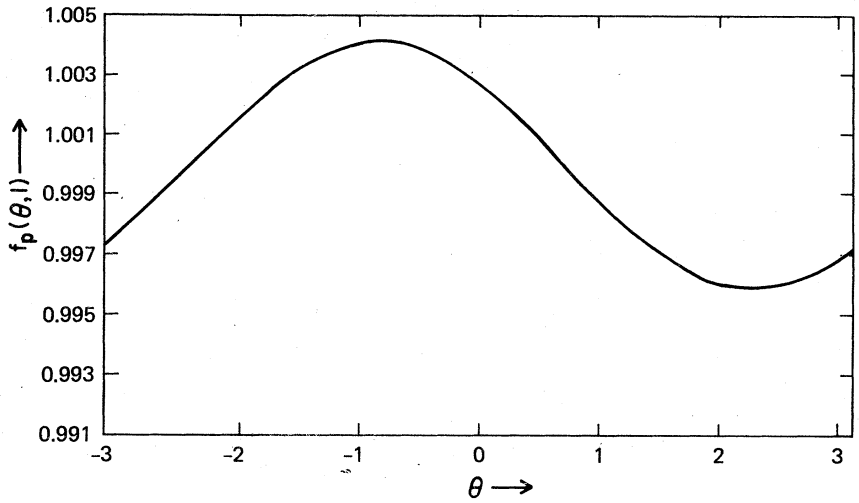

FIG. 12. Plot of the phase distribution function vs the phase θ for the small-signal ($\epsilon=0.1$, $\mu=2.6$) maximum-gain case.

$$\left.\frac{d\zeta}{d\zeta_0}\right|_{\zeta_{0n}} = 2\,\mathrm{dn}\left(w,\frac{1}{k}\right)\left\{\frac{k\epsilon}{\mu}+\frac{\sin\zeta_0}{4k}\left[\epsilon\tau+\frac{1}{k}F\left(\frac{\zeta_0}{2},\frac{1}{k}\right)\right]-\frac{1}{k^2-1}\left[kE\left(\frac{\zeta_0}{2},\frac{1}{k}\right)-\frac{\epsilon\sin\zeta_0}{\mu}\right]\right\}, \tag{4.19}$$

to be used in (4.16).

Case 2: $k^2<1$. By (2.37), we need roots of

$$\tan\tfrac{1}{2}\theta=\frac{k\,\mathrm{sn}(u,k)-\mathrm{dn}(u,k)\tan\frac{1}{2}\mu\tau}{\mathrm{dn}(u,k)+k\,\mathrm{sn}(u,k)\tan\frac{1}{2}\mu\tau}\,. \tag{4.20}$$

By (2.37) we obtain

$$\left.\frac{d\zeta}{d\zeta_0}\right|_{\zeta_{0n}} =\frac{1}{2k}\,\mathrm{cn}(u,k)\left\{\frac{\mu}{\epsilon}+\sin\zeta_0\left[\frac{1}{1-k^2}\left(E(\phi_0,k)-\frac{\mu}{2\epsilon}\tan\frac{\zeta_0}{2}\right)-F(\phi_0,k)\right]\right\}+\frac{\sin\zeta_0}{2k}\,\frac{\mathrm{sn}(u,k)}{\mathrm{dn}(u,k)} \tag{4.21}$$

for use in (4.16).

In Fig. 12 we plot $f_p(\theta,\ \tau=1)$ for the small-signal maximum-gain case ($\epsilon=0.1$, $\mu=2.6$). It agrees with the approximate analytic result of Ref. 6 to 4–5 significant figures. At $\tau=0$, it is normalized to unity and is uniform. Figure 13 for $\epsilon=0.5$, $\mu=2.6$ is essentially the same, with larger amplitude variations. (Note change in vertical scale.) In Fig. 14 we have plotted (4.20), viz., θ vs ζ_0, both from the exact solutions (dotted curve) and from the approximate analytical results of Ref. 6 (solid curve) for $\epsilon=0.5$ and $\mu=2.6$. In the small-signal regime, θ is a monotonically increasing (approximately linear) function of ζ_0. So, for each θ there is only one ζ_{0n} to contribute to $f_p(\theta,\ \tau=1)$. Again, Fig. 13 was plotted from exact root, ζ_0 for fixed θ obtained in Fig. 14 for the same ϵ and μ (open orbits).

We again note by comparison with (4.19) and (4.21), discontinuities in f_p will occur when we go from open to closed orbits. This occurs near $\theta=0$ in Fig. 15 for $\epsilon=2.0$, $\mu=3.0$. In Fig. 16 we have plotted θ vs ζ_0, and we see that the change in the number of roots ζ_{0n} for fixed θ changes near $\theta=-1$ and $\theta=-1.3$, accounting for these two discontinuities in $f_p(\theta,\ \tau=1)$ in Fig. 15. Similar re-

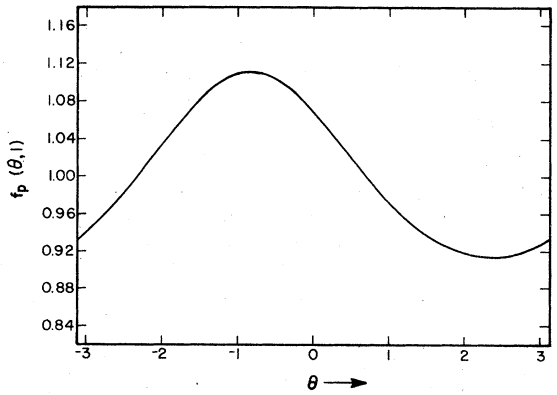

FIG. 13. Plot of phase distribution vs phase for $\epsilon=0.5$ and $\mu=2.6$. Note change in vertical scale from Fig. 12.

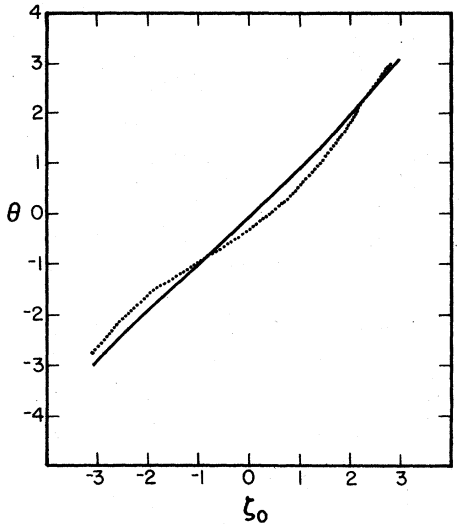

FIG. 14. Plot of final phase vs initial phase for $\epsilon = 0.5$ and $\mu = 2.6$. Solid curve is approximate analytical result and dotted curve is exact result.

marks apply to Figs. 17 and 18 for $\epsilon = 3$, $\mu = 3.9$. The nice "sinusoidal"-type distributions for weak field (small ϵ) develop spikes at higher operating levels, as seen in Fig. 17.

V. CONCLUSIONS

Although discontinuities are present in both the energy and phase distributions, they have no apparent effect on the gain-saturation calculation.

It is apparent from Fig. 3, that the saturation mechanism is different from an ordinary laser since, as we pump harder, an increase in gain may still be achieved by varying the detuning by

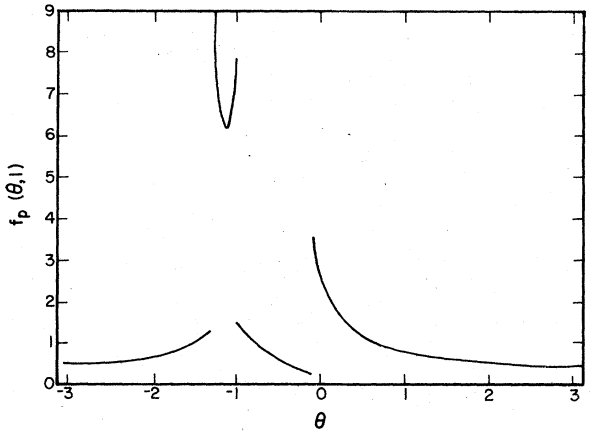

FIG. 15. Phase distribution function vs θ for $\epsilon = 2.0$ and $\mu = 3.0$. Discontinuity near $\theta = 0$ is due to k changing from less than 1 to greater than 1. The discontinuities near $\theta \cong -1$ and -1.3 are due to changes in number of roots (see Fig. 16).

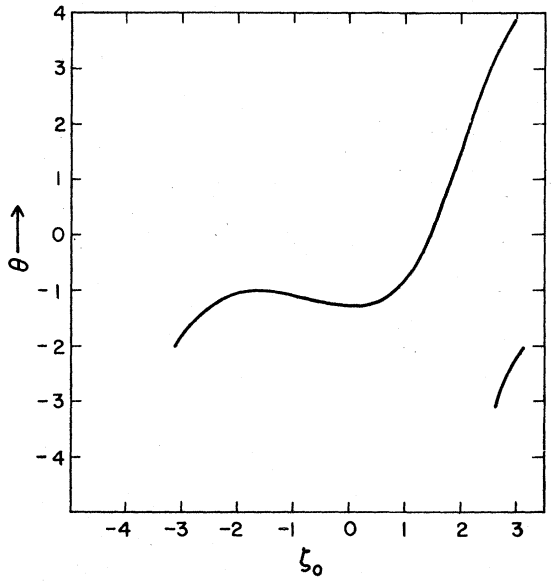

FIG. 16. Final phase vs initial phase. The discontinuous change in the number of roots from 1 to 3 of ζ_0 for fixed θ at $\theta = -1$ and -1.3 is clearly evident.

virtue of the asymmetry developed in the electron energy distribution function.

Gain has been calculated using a narrow energy electron distribution and a uniform phase distribution (the so-called small-cavity limit). Since the use of storage rings is envisioned for future applications, the effect of the energy and phase discontinuities as well as the effects of space charge and losses due to synchrontron radiation must be carefully considered.

In typical operation with small-cavity losses, the laser-cavity fields should grow until the electrons evolve into the closed-orbit region and sat-

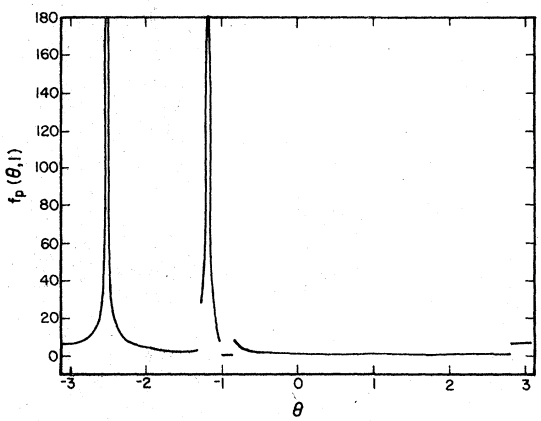

FIG. 17. Electron-output phase distribution vs θ for $\epsilon = 3$ and $\mu = 3.9$. Number of roots changes at $\theta \sim -1.0$, while k changes from less than 1 to greater than 1 at $\theta \sim -1.3$.

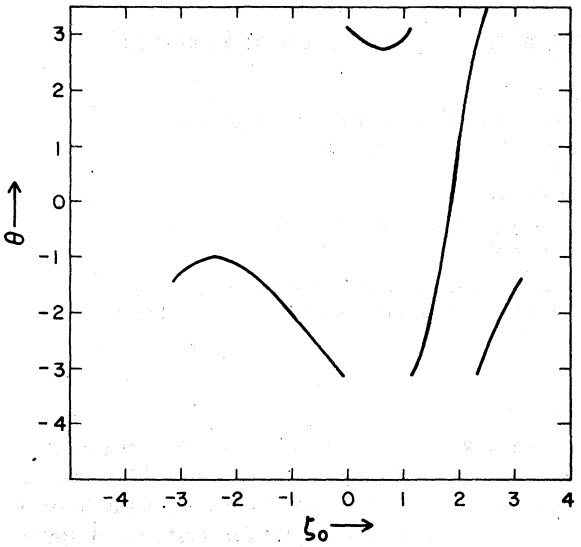

FIG. 18. Final phase vs initial phase for $\epsilon = 3.0$ and $\mu = 3.9$. The abrupt changes in the number of roots which contribute to the phase distribution at $\theta \cong -1.0$ is evident. The discontinuities of θ vs ζ_0 are due to the computer picking the principal values of (4.17b) or (4.20).

uration occurs. We therefore expect that a realistic description of a free-electron-laser oscillator would require analysis of the closed orbit region as presented here. The pendulum phase-space approach seems to be very useful in obtaining physical insight into the physics of the free-electron laser.

Finally, we wish to emphasize the importance of the "bunched" electron beam produced by the free-electron laser. This analysis shows how an external laser may be used in combination with a static periodic magnetic field (or incoming microwave field) to modulate coherently a relativistic electron beam at optical wavelengths. Such a beam may be used to drive a high-gain optical klystron[11]; other application and the importance of such a beam are reviewed in Ref. 11. The dispersive effects of energy spread in a relativistic electron beam are suppressed because all particles travel at approximately speed c. This allows transport of optical information by the electron beam over reasonable distances.[12] A scattering process, sensitive to electrons, which is resonant at the modulation frequency, may be enhanced under the proper conditions and made proportional to the square of the electron flux[13] Such an effect will be an observation of a collective scattering process which depends on the shape of the electron wave packet.

ACKNOWLEDGMENTS

One of us (W.H.L.) is deeply indebted to Dr. Keith Boyer of Los Alamos Scientific Laboratory for stimulating his interest in this problem and his support of this work, as well as the support of the Applied Photochemistry Division of the Los Alamos Scientific Laboratory, as a consultant. He is also indebted to Dr. J. P. Harris of the NSF for his support of this work. We wish also to thank John A. Dentinger for the computational work. This work was supported in part by the NSF under Grant No. ENG-76-23704 and by U.S. Army Contract No. DASG60-77-C-0083.

*Consultant to University of California, Los Alamos Scientific Laboratory.

[1]J. D. Jackson, *Classical Electrodynamics* (Wiley, New York, 1962).
[2]W. B. Colson, Phys. Lett. A 59, 187 (1976); Ph.D. thesis (Stanford University, 1977 (unpublished).
[3]H. Motz, J. Appl. Phys. 22, 527 (1951); H. Motz, W. Thon, and R. N. Whitehurst, *ibid.* 24, 826 (1953).
[4]L. R. Elias, W. M. Fairbank, J. M. J. Madey, H. A. Schwettman, and T. I. Smith, Phys. Rev. Lett. 36, 717 (1976); Phys. Today 17, No. 2 (1976).
[5]D. A. G. Deacon, L. R. Elias, J. M. J. Madey, G. J. Ramian, H. A. Schwettman, and T. I. Smith, Phys. Rev. Lett. 38, 892 (1977); Sci. Am. 63, No. 6 (1977).
[6]W. B. Colson, in *Physics of Quantum Electronics* (Addison-Wesley, Reading, Mass., 1977), Vol. 5, Chap. 4; Phys. Lett. A 64, 190 (1977).
[7]F. A. Hopf, P. Meystre, M. O. Scully, and W. H. Louisell, Opt. Commun. 18, 413 (1976); F. A. Hopf, P. Meystre, M. O. Scully, and W. H. Louisell, Phys. Rev. Lett. 37, 1342 (1976).
[8]J. M. J. Madey, J. Appl. Phys. 42, 1906 (1971).
[9]N. M. Kroll and W. A. McMullin, Phys. Rev. A 17, 300 (1978).
[10]F. A. Hopf, P. Meystre, M. O. Scully, and W. H. Louisell, Phys. Rev. Lett. 39, 1496 (1977).
[11]C. K. Chen, J. C. Shippard, M. A. Piestrup, and P. H. Pantell, J. Appl. Phys. (to be published).
[12]L. D. Favro, D. M. Fradkin, P. K. Kao, and W. B. Rolnick, Appl. Phys. Lett. 19, 378 (1971).
[13]L. D. Favro, and P. K. Kao, Phys. Rev. D 3, 2931 (1971).